

FORCE AND DEFORMATION MODELING OF THE FLAPPING WING: *CALLIPHORA VICINA*

M.N.M. Nasir^{1,2}, Fritz Olaf-Lehman³, Stanislav Gorb

¹Department of Aeronautics, Universiti Teknologi Malaysia, Malaysia

²Department of Aerodynamics, Technical University of Delft, Netherlands

³BioFuture Research Group, University of Ulm, Germany

⁴Max Planck Institute in Stuttgart, Germany

ABSTRACT

There is a description since several decades ago those insects have evolved that an extra lift is obtained due to the rotational and translational mechanism especially during stroke reversals. Nonetheless, this issue is strongly depending on the consequences of the wing stroke kinematics prescribed. Another issue to be concerned is the inertial force created due to the rapid acceleration or deceleration by its own distributed mass. Most people found that the force exerted to the insect's wing mostly comes from the inertial force but no one has been able to list down all the reacted forces including aerodynamic force, Magnus force and added mass effect. Subsequently, a simulation model will be made to integrate all the relevant forces in term of magnitude and direction to find a clean single force named as a resultant force. Several years ago, majority of the wing deformation analysis discussed are base on the certain forces and none of them analyze it by considering all the forces which possibly involved. Therefore, the deformation characteristics will be calculated based on the elemental stiffness data depends on the pattern of supporting three dimensional insect's wing architecture that will be subjected to all the forces which perhaps involved. The resultant force will be accurately dispersed in spanwise direction according to chord length and the wing mass distribution in order to obtain an accurate wing deformation characteristic depending on local wing's flexural stiffness.

Keywords: *Calliphora Vicina, wing deformation, inertia, added mass, Magnus force, wing stiffness.*

*Corresponding author : aeronazri@yahoo.co.uk

1.0 INTRODUCTION

Since a couple of years, biologists are trying to get a better insight and understanding of the locomotors system of the flapping insect by using unsteady quasi-aerodynamic. As the scientific community increased, engineers start to realize that the flapping wing insect inspire to the development of Micro Aerial Vehicles at low Reynolds numbers as well as the low viscosity environment. As a result, there are several new ideas and observation method to study the flapping behavior such as robotic model, Computational Fluid Dynamics (CFD) computer simulations, high speed camera, and Digital Particle Image Velocimetry (DPIV) technique. These sophisticated methods and techniques are used to increase the understanding of the flapping flight and these new development has significantly help the biologists to carry out their research.

Most of the researchers estimate the real or generic flapping wing by using experiments and computational simulations. Therefore, the present study is performed in order to validate and to compare all the significant effects from various different methods and variables involved that may produce forces towards flapping wings. This has lead to the following questions of how significant of all the forces reacted on the flapping wing in term of priority (ranking) and how critical they are at certain period of time depending on the operating condition. In order to answer these questions, the following scopes and objectives have to be defined. Several MATLAB models have been implied in order to calculate all the reacted forces and show the role of each variable. As they act simultaneously, then all the acting forces subjected will be plotted and ranked to verify their significance.

Lately, the common analysis and observation of the wing deformation of the flapping insect are based on the certain forces such as Ennos [1] in term of wing inertial force, Dickinson *et. al* [2] in term of aerodynamic force and so on. Possibly, it can be a good stepping point for the observation of the flapping wing deformation but it is not fully accurate because all the forces explained before such as aerodynamic forces, inertia forces, Magnus force and added mass effect are acting simultaneously because they will never stand alone. Therefore, a simulation models using the Walker model [3] will estimate the forces acting on a blowfly (*Calliphora Vicina*) wing and also associate all the relevant forces in term of magnitude and direction named as resultant force. In addition, this is an appropriate way to observe the effect of the environment variation especially in term of force interface because every single force developed may be affected by the change of surroundings for instance, air density.

2.0 EXPERIMENT, MEASUREMENT AND IMPLEMENTATION

An insect wing consists of a three-dimensional skeletal network of relatively hard veins, which are interconnected through thin membranous areas called cells [4]. These structures consist of cuticle, a biological fibrous composite material [5] whose mechanical properties range from very stiff to flexible [6]. The leading edge of the wing is comprised of a very stiff structure with three dimensional reliefs in order to provide high rigidity to the span of the wing. The serial elastic

elements of the wing may act as dampers of an aerodynamic force subjected to the wings, which are responsible for gradual twisting of the leading edge [3]. Presumably this mechanism is an essential adaptation for the highly maneuverable flight, especially in the condition, when unstable wind pulses act on flying insect. For instance, the Ultralight airfoils (generally only 0.5-5 percent of body mass) will be able to withstand the forces subjected upon them by the surrounding air, as well as the inertial forces caused by accelerating and decelerating mass up to several hundred times per second [7].

The Figure 1 shows the microscopic view of the blowfly wing that will be used later to obtain the stiffness along the wing span. The wing is divided into seven strips from wing root based on venation patterns. Since biological system are considerably scattered, ten freshly killed male blow flies are used for each measurement.

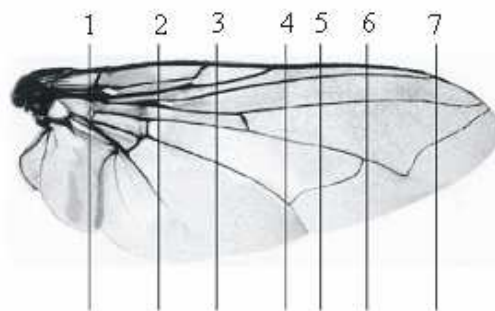


Figure 1: Magnified view of a blowfly wing (Ganguli et. al, 2008)

Performing measurements of flexural stiffness (EI) averaged over the whole wing is relatively straight forward [7, 8], but measuring spatial variation in flexural stiffness throughout a wing is more challenging. Therefore, the study begins with the experiment and the analysis of mechanical properties of the wing (Figure 1). The experiment to determine the stiffness variation along the wing of the blowfly was performed by Ganguli [10]. The spring constant of each insect is unique and it is depending on the size, species, and environmental effect and so on. Therefore during the experiment, several samples need to be tested and the average value calculated in order to determine the mean value and to understand the ordinary scenario.

Next, the kinematics behavior of the wing will be studied in detail and visualized by modeling codes. The real behavior of the dynamic flapping wing in term of aerodynamic force generation and all the features involved will be calculated. In the modeling code, the wing will be modeled as a dynamic object with a translating and rotating trajectory in order to determine the aerodynamic force of the flapping flight. Furthermore, the velocity and the acceleration of the wing translation will be plotted because these characteristics are vital for the inertial effect and so on. The most essential topic to be talked about is the location of where those characteristics hit the maximum points in time trace because they can help us to locate the exact location of the remarkable wing deformation. The Unsteady Blade Element (USBEL) method introduced by Walker [11] will be

implied in order to compute the presence of the dynamic force of the lift and drag force. The aerodynamic force of the flapping flight will be plotted in time domain and also the important of the wing rotational effect will be evaluated in detail together with the force scaling method.

Afterward, the inertial force of horizontal and vertical direction simultaneously with the secondary forces which include the Magnus force and added mass effect will be calculated in order to verify it's significant with respect to each other. By inspiring from Ennos [1] ideas that the inertial force is the most dominant aspect that may cause the wing deformation, several investigations will be carried out. The formulas and algorithms involve will be listed simultaneously with the mass distribution in spanwise direction from the wing root up to the tip. Even though some people may assume that the secondary forces are not vital, but for this study, this issue also had been coded in the modeling for the verification. Accordingly, the inertial forces and the secondary forces will be plotted in time trace to clarify the forces distribution in time domain and specify the moment where they turn out to be very important especially during wing stroke reversal.

Finally, all the forces will be plotted in a same graph in order to rank them and to observe the significant with respect to that particular situation. Then, they will be integrated or associated and the relationship between them will be analyzed. Most of the previous researchers calculated all the relevant forces but no one is willing to figure out the correlation between all the subjected reacted forces. By using an accurate resultant force, we will be able to calculate an accurate wing deformation by considering relevant aspects of operating conditions. The potential energy due to the wing deformation will be explained in detail and it's important towards the wing performance.

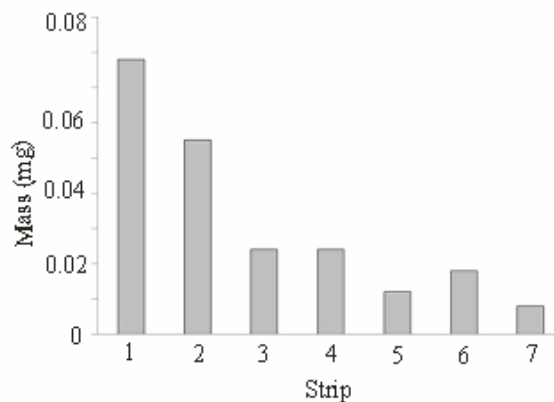


Figure 2: Variation of wing mass in spanwise direction

2.1 Flexural stiffness analysis

Since biological system are considerably scattered, ten freshly killed male blowflies are used for each measurement. The average total body weight of the fly is approximately 59.0867 mg. The weight of the ten species may vary as low as from 44.0523 mg to as high as 76.2182 mg with a standard deviation of 10.2097 mg. The mass measurement was performed by using a UMX2 weight scale

manufactured by Mettler Toledo and capable of measuring up to 0.1 μg . Both wings of ten flies are considered resulting twenty wings in total. The calculated average weight of the wing is 238.7 μg (approximately 0.4 percent of the total body weight). According to the measurement high mass mostly concentrated at the region near the wing root where the distribution of vein and join is high as shown in Figure 2. The next step is to define the total length of the wing and also the location for every single section from wing root. A Mitutoyo precision microscope was used to measure the length of all the seven sections used in order to quantify them as an engineering beam. Based on the measurement carried out the wing length ranged from a minimum of 7.46 mm to a maximum of 9.30 mm and the average length is 8.42 mm. The width ranges from a minimum of 3.07 mm to a maximum of 4.038 mm with an average width 3.61 mm.

2.2 Flapping wing kinematics

In this chapter, we will consider a dynamic model which be able to describe the wing as rotating and translating object instead of just rigid at certain given location in the coordinate grid according to the kinematic prescribed. Besides, Shvets et. al [15] classify insect flapping flight according to the flight trajectory and recognized three main flight types, forward flight, hovering, and flitting (the mixture of the first two).

Name	<i>Calliphora Vicina</i>
Wing length, R	0.00842m
Average wing chord, c	0.00361m
Average wing area, S	$6.07924 \times 10^{-5} \text{m}^2$
Aspect ratio, b^2/s	4.6648

Figure 3: The wing data and characteristic of the blowfly

As a first approximation, wings can be considered to translate in a plane containing the wing hinge called stroke plane. Normally, it is perpendicular to the longitudinal body axis and is inclined to the body axis to the angle from 30 degree to 60 degree. While hovering, the stroke plane may reach approximately close to the horizontal axis [6]. The stroke begins at the start of the downward wing movement from the highest point of the wing trajectory.

Stroke cycle asymmetric in several aspects and in order to adjust the angle of attack, the wing have to rotate about their longitudinal axis. Moreover, an incline stroke plane appears as a second features for many insect because it strengthens the stroke symmetric especially during straight flight where the generated force are significantly during down stroke and will diminished in the upstroke. Basically, there are three different angles that representing the wing kinematics which are stroke angle ϕ , angle of attack α and heaving angle θ . Later, we will be able to adjust these features in the modeling code in order to see the significant of each variables with respect to the wing kinematic used. The Robofly kinematic style will be used in the modeling because this is the only data accessible by

researcher even though the flexural stiffness obtained before is belonging to *Calliphora Vicina*. However, it is not a vital issue because our model is not related with any specific species and it can be modified later according to specific case and situation.

The Figure 4(A) explains the stroke angle where the maximum value of the angle is approximately 90 degrees upward and 70 degrees backward. According to the first graph it is clearly describes that the wing start its trajectory approximately near the maximum angle at the back and gradually move the wing forward to the front position before it does the downstroke and turn back to the original position. For further clarification especially during the stroke reversal transition, the modeling performs the upstroke and downstroke plotted twice especially to observe the transition region between the two wing strokes. The Figure 4(B) is the wing stroke velocity where it clearly shows that the stroke velocity turns to maximum point near the mid stroke position meanwhile Figure 4(C) describes the wing stroke acceleration where the maximum acceleration located exactly at the end of the wing stroke just before it change the direction on the opposite site called wing stroke reversal. The vertical line plotted in this graph described the exact location of the stroke reversal occur at the highest point of the wing trajectory.

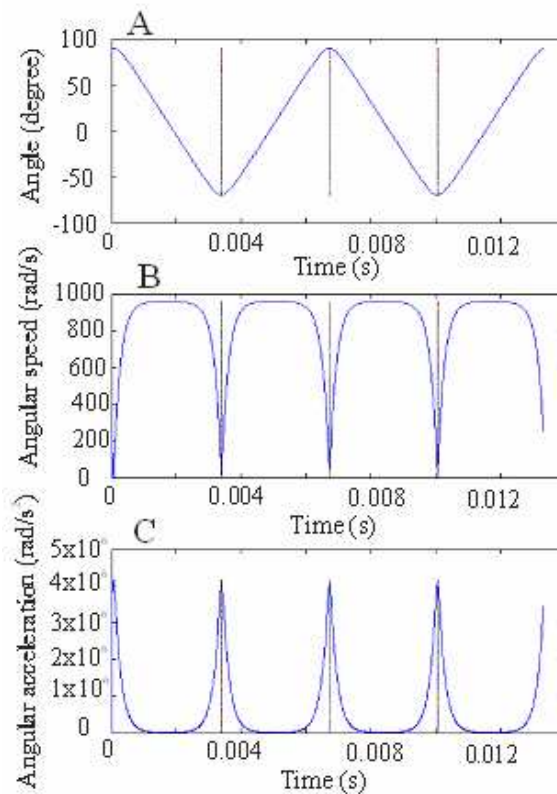


Figure 4: (A) Wing stroke angle ϕ , (B) Wing stroke angular velocity $\dot{\phi}$ and (C) Wing stroke, angular acceleration $\ddot{\phi}$

The term of wing rotation is generally refers to the change of angle of attack around a chordwise axis. This scenario might occur along the stroke plane; however it will be tremendously happened during stroke reversal as the wing stroke trajectory change the direction. During the downstroke - to - upstroke transition, the wing supinates quickly and a rotation will bring the ventral surface of the wing upwards. The wing will pronate quickly at the end of upstroke bringing the ventral surface to face downwards.

Figure 5(A) explains about the wing rotation angle which plays an important role in order to define the correct lift and drag coefficient at certain angle of attack according to the equation given by the plotted lift-drag curve. The trend of the graph is looked saw tooth liked shape. There are two different colors used to distinguish the way between the rotation angle with respect to the vertical axis (blue) and the rotation angle with respect to horizontal axis (green). The wing rotation angle with respect to vertical axis is vital to describe the stroke angle of real insect whereas the wing rotation angle with respect to horizontal axis is significant to determine the aerodynamic coefficient of lift and drag force.

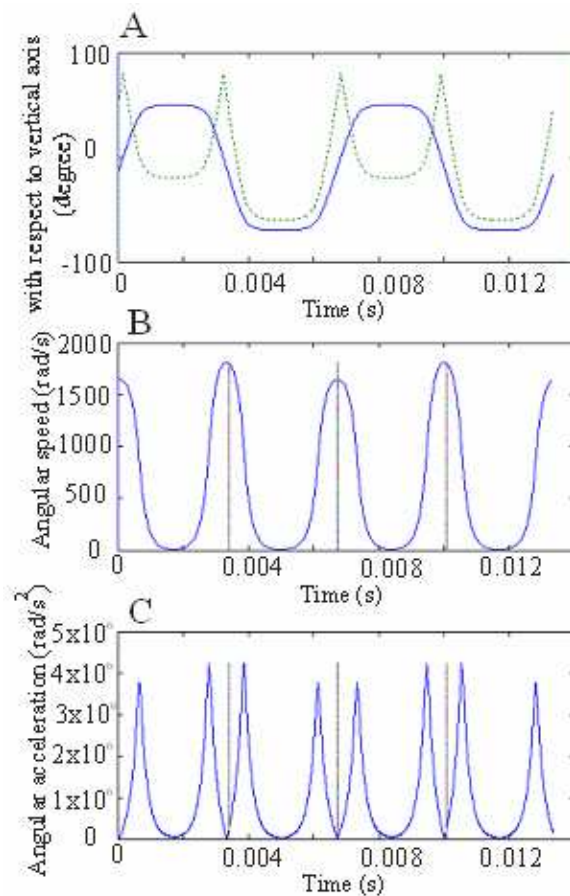


Figure 5: Wing rotation angle α , Wing rotation angular velocity $\dot{\alpha}$ and Wing rotation angular acceleration $\ddot{\alpha}$

The Figure 5(B) shows the wing rotation angular velocity which the maximum velocity again occurs near the wing stroke reversal in both side (upward and downward). The Figure 5(C) describes the wing acceleration for wing acceleration. Here, the acceleration turns to maximum just after and before perform the stroke reversal. However, in between them the acceleration rapidly turns to zero and jump back to hit the maximum point near the wing stroke reversal. The vertical line plotted in this graph described the exact location of the stroke reversal occur at the highest point of the wing trajectory.

2.3 Aerodynamic forces

The main principle of the force generation has much in common in all the flapping creatures for instances flying and swimming animals. They were considered in several literatures of animal aerial and aquatic locomotion [7, 12]. Even though this theory is not being able to describe all the phenomena observed in nature but it is clearly facilitates research and suggesting various mechanism that might be helpful to explain the force generation especially regarding to aerodynamic force that will be explained in further detail in this chapter. The flight force are further enhanced with respect to the ordinary fixed wing due to the involvement of other mechanism acting during their rotation (change in angle of attack) especially at the stroke reversal and also the wing-weight interaction (13). In this study, we will investigate the involvement of all the enhancement effect especially during the wing stroke reversal by using the Unsteady Blade Element (USBE) method invented by Walker [11] that will be broadly used in our models.

Furthermore the effect of rotational circulation also will be plot in the graph in order to see it's significant. Dickinson et al. [5] firmly believed that the present of two rotational force peaks occurred due to this effect. The wing rotation believed as one of the source circulation that provide the upward force that can be part of enhancement in aerodynamic lift performance.

The Unsteady Blade Elements, USBE model is a good method to define all the forces reacted and a good measurement to compare with Computational Fluid Dynamic (CFD) modeling and the experimental robotic modeling result. According to Walker [16], the theoretical force acting on the flapping wing, per unit span on a thin airfoil at certain angle of attack is the function of the four circulatory component (translational circulation due to wing attached to a translating body, heaving circulation due to the wing active or passive oscillation, rotational circulation around the spanwise axis and Magnus circulation) plus added mass effect which is normally small for low density ambient air. As usual, the USBE model starts with some description on the flapping wing kinematics as described. Therefore, the developed models will be able to cope with any given wing kinematics and wing positions during the wing movements at certain time domain.

The polar graph [14] plotted represents the lift coefficient versus the drag coefficient at various different rotation angles. It is a good guidance to explain the generation of the aerodynamic force as the wing rotates in a spanwise axis. This semi circle polar graph is not similar to the ordinary polar graph of a fixed wing because in this case the angle of attack beyond the stall angle also takes into

account. It happens because in a flapping flight it will never stall forever unless it inclined below the stroke axis (negative angle of attack). As further analysis done, this trend shown in a polar graph can be summarized and simplified by the mathematical equation it is very useful to be put in the analysis.

2.4 Inertial forces

Most of the previous research assumed the wings are moving in simple harmonic motion [1]. However, not every single insect can fly by simple harmonic motion because some of them have their own natural flapping kinematics. For instance, in time domain, several insects have a quick and a sharp turn of wing stroke reversal that may cause inertia whilst others might be acting differently and take a longer period of time. Numerous researchers for instance Ennos [1] believed that inertial forces for instance are more significant than aerodynamic force (lift and drag) and secondary force (Magnus force and added mass effect).

During flapping flight, animal invest power to move in the air in order to produce the aerodynamic forces to keep them aloft and moved the wing due to the inertial forces. The moment of inertial is small when the mass is low and would concentrate near the axis rotation (wing root). In this study, the moment of inertial will be determined by using the wing strip analysis which is the continuation of Walker's [11] USBE method explained. The inertia effect is crucial due to the rapid acceleration and deceleration especially during stroke reversal. Therefore, if this effect combined together with the aerodynamic force, they will generate more accurate combination force that will involve in wing deformation. Be aware, the rapid acceleration and deceleration are not only composed of wing stroke motion but it also includes the wing rotation simultaneously. Therefore, in this case these two wing motions will produce two different kind of inertial force that will be acting in different axis (vertical and horizontal axis).

In this analysis, the wing does not only flap in the stroke direction but it can also rotate with respect to the rotational axis. Therefore, the inertial force will be isolated into two different components which are vertical and horizontal axis. The contribution of inertial effect towards the wing deformation may be varied along the wing. Consequently, prior the calculation the distribution of mass with respect to the distance of wing based have to be determine. Apart of the investigation of the magnitude of the inertial force, the distribution of the mass also will be defined prior the analysis in order to ensure the mass obtained from the strip analysis can be distribute accurately.

Let's us investigate the moment set up in an arbitrary wing strip located at distance r from the wing base. Each wing strip has a mass of dm with a distance r from the wing base when the wing subjected to an angular acceleration either due to the wing stroke or due to the wing rotation. According to Ellington [7], the inertial forces during the flapping flight in horizontal direction are proportioned to the integration of the first moment of wing mass element in each strip,

$$dF_h^*(t) = l_{x_n} \dot{\phi} dm_{w_n} \quad (1)$$

During the wing movement, it does not only exert to the inertial force in horizontal direction due to the wing movement along the stroke plane but also to the inertial force due to the change of wing rotation (angle of attack) in vertical axis. Inertial force associated to acceleration in the vertical plane due to wing rotation;

$$dF_v(t) = l_{y_n} \ddot{\alpha} \cos \alpha dm_{w_n} \quad (2)$$

The inertial force produced during the wing rotation in the horizontal plane;

$$dF_h(t) = dF_h^*(t) + l_{y_n} \ddot{\alpha} \sin \alpha dm_{w_n} \quad (3)$$

2.5 Magnus force and added mass effect

Magnus effect is described as a physical event of a spinning object that would produce a whirlpool of rotating air about itself. According to Bernoulli's principle, the pressure is lower on the side where the velocity is greater. Consequently, there is an unbalanced force at right angle to the wind. This is what we called Magnus force. In the case of flapping wing, as the insect rotates its wing during the wing stroke, it also will subject to the Magnus effect simultaneously. In addition, the modeling simulation also concern about the density change that strongly influences the Magnus effect calculation. Therefore, the model will indicate the variation Magnus force amount as several variables would change depending on the working environment.

The following equation demonstrates the manipulation of characteristic needed to determine the Magnus force by Walker [11].

$$dF_m(l_x, t) = \frac{1}{4} \rho \pi c^2 (l_x) \dot{l}_x R \dot{\alpha}^2 dR \quad (4)$$

In addition, the effect of added mass is usually not significant when compared to the aerodynamic force and inertial force especially in a low density operating condition. Added mass is the inertia added to a system because a rapid acceleration and deceleration, a body has to move some volume of neighboring fluid as it travels through it. Furthermore, it happens because the object and the fluid cannot occupy the same physical space at the same time. In a simpler way of explanation, it can be modeled as some volume of fluid moving with the object, though in reality, it will be accelerated to various degrees.

Walker (2002) described the added mass force in his USBE method as an acceleration reaction normal to the wing element,

$$dF_a(l_x, t) = \frac{1}{4} \rho \pi c^2 (l_x) \dot{v}_n(l_x, t) \beta_n dR \quad (5)$$

2.6 Forces integration

Majority of the analysis and observation of the wing deformation are based on the certain forces such as Ennos [15] in term of wing inertial force, Dickinson *et. al*

[2] in term of aerodynamic force and so on. Possibly, it can be good preliminary studies for the observation of the flapping wing deformation but it is not fully accurate because all the forces are acting simultaneously because they will never stand alone. The simulation model will continue the analysis in how to associate all the relevant forces in term of magnitude and direction and find a clean single force named as resultant force. All the related forces acting in the horizontal direction will be compiled and further judgement in horizontal direction will be made. Basically, there are two forces acting in this direction which are horizontal inertial force and drag force. Surprisingly, at certain moment they are acting simultaneously in the same direction or vice versa. Therefore, in this section, not only the magnitude of the forces will be taken into account, but the direction also will be considered accurately during the upstroke and downstroke as well.

During the downstroke position, the wing moves forward while the drag always acts on the opposite direction of motion (backward). However, the horizontal inertia is totally different because it is depending on the acceleration or deceleration of the wing stroke as stated in the previous graph. Acceleration starts from zero and will turn to maximum point at the stroke reversal before it eventually decreases reach approximately to origin at the middle of the wing stroke. Accordingly, the horizontal inertial also start to react on the similar direction of the drag and rapidly change the direction to the opposite direction just after passing the mid-stroke point.

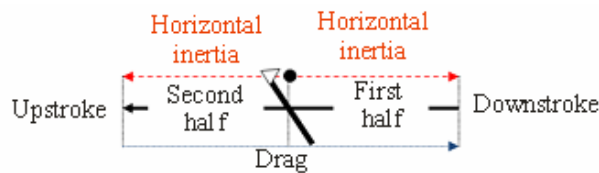


Figure 6: Schematic diagram of wing downstroke

The following equation is the formula that can be used to exact value of resultant force in horizontal direction based on the situation and the location of the wing stroke as explained before.

For the first half of wing stroke,

$$dF_{Th}(t) = dF_h(t) + dD(t) \quad (6)$$

For the second half of wing stroke,

$$dF_{Th}(t) = dD(t) - dF_h(t) \quad (7)$$

Similarly, during the upstroke position, the wing moves backward while the drag always acts on the opposite direction of motion (frontward). Again, the horizontal inertia is acting depending on the acceleration or deceleration of the

wing stroke. Basically, the idea to calculate the resultant force is almost the same as the downstroke motion where the drag always acting opposite of the wing motion (forward). Therefore, the horizontal inertial also start to react on the direction of the drag and rapidly changes the direction to the opposite direction just after passing the mid-stroke as the wing stroke acceleration steadily reduce.

According to the Figure 7, let assume the wing at certain angle of attack, α move in the horizontal direction. As usual, lift, L will acts perpendicular to the oncoming flow direction whereas drag, D always opposes the relative motion and they cause the aerodynamic force, F_A as the resultant force as shown in equation 9. The aerodynamic force has some angle with respect to the x -axis denoted as θ . Furthermore, with the appropriate values of angle of attack, angle of aerodynamic force and its magnitude, we can simply calculate the vertical force, F_{A_v} due to the aerodynamic effect which acting perpendicular to the wing as shown in Figure 7.

$$\theta = \tan^{-1} \frac{dL}{dD} \quad (8)$$

$$dF_A(t) = \sqrt{(dL(t))^2 + (dD(t))^2} \quad (9)$$

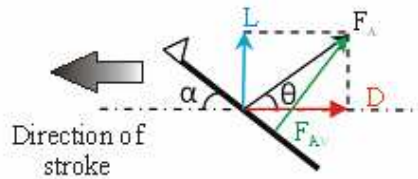


Figure 7: Schematic diagram of aerodynamic forces acting in vertical direction

$$dF_{A_v}(t) = dF_A(t) \tan(\theta + \alpha) \quad (10)$$

During the wing rotation, the trailing edge wing will rotate with respect to the leading edge as the rotational axis. Accordingly, the leading edge stays for few seconds at the most forward or the most backward position along the stroke axis while the trailing edge rotates with respect to the rotational axis. Therefore, the distribution of the inertial force is more concentrated at the leading edge or in a simple assumption in this case the resultant vertical inertia force only reacted at the leading edge.

In this case, the wing rotates anticlockwise with respect to leading edge rotational axis. In the first half of the rotation, the resultant inertia force will reacted upward in the direction of lift force whilst in the second half of the rotation the resultant inertia force will also reacted in the same direction of the lift force. This is happened because the angular acceleration of the wing rotation is gradually increases and consequently changes the direction during the second half rotation.

Bear in mind that Magnus force acting in the same direction of lift force whereas added mass effect is always stand normal to the wing element [16].

Furthermore, all the related forces acting in the vertical direction will compile and further judgement in vertical direction will be done. Astonishingly, at certain moment they are acting simultaneously in the same direction or vice versa. Meanwhile, in this section, not only the magnitude of the forces will be emphasized, but the direction also will be considered accurately during the upstroke and back stroke as well. Nevertheless, there are another two forces that might be acting in the same direction (vertical direction) which are in Magnus force and added mass effect.

$$dF_{T_v}(t) = dF_{A_v}(t) + dF_a(t) + dF_m(t) \quad (11)$$

Finally, the resultant of the total force is,

$$dF_{T_r}(t) = \sqrt{(dF_{T_h}(t))^2 + (dF_{T_v}(t))^2} \quad (12)$$

2.7 Wing deformation

The resultant force obtained is the most accurate value of force that can be implied for the wing deformation by using Hooke's Law. In this section, wing will be modeled as a beam that is completely fixed at one end and completely free at the other. The deflection characteristics of the beam will be calculated based on the elemental stiffness data calculated in the previous chapter. Moreover, the resultant force will be accurately dispersed in spanwise direction according to chord length and the wing mass distribution in order to get an accurate answer.

Deflection is a term used to explain the degree to which a structural element is displaced under a certain amount of load. The elemental elastic deflection of a cantilever beam (free at one end), can be calculated using:

$$d\delta_n = \frac{dF_n}{dk_n} - d\delta_{n-1} \quad (13)$$

The elemental angle of deflection of a cantilever beam (free at one end), can be calculated using:

$$d\theta_n = \tan^{-1} \frac{d\delta_n}{dl_{x_n}} \quad (14)$$

2.8 Elemental elastic potential energy

Elastic potential energy is potential energy stored as a result of deformation of an elastic object. It exists when there is a force that tends to pull an object back towards some original position when the object is displaced. It is called potential energy because it has the potential to be converted into other forms of energy,

such as kinetic energy, and to do work in the process. The standard (SI) unit of measure for potential energy is Joule, the same as for work or energy in general. It is equal to the work done to deflect the beam, which is depends upon the spring constant, k as well as the beam arm length,

The following equation explains the way to calculate the elementary elastic potential energy, E

$$dE_n = \frac{1}{2} dk_n d\delta_n \quad (15)$$

3.0 RESULTS

3.1 Flexural stiffness

The Figure 8 shows the distribution of the spring constant along the span. The graph proved that the assumption made by Combes and Daniel [9, 14] that the stiffness distributions in spanwise direction are exponential trend is true. Clearly from the graph we can say that the high spring constant concentrated near the wing root region up to 42.84N/m due to the high distribution and thicker vein near certain particular location.

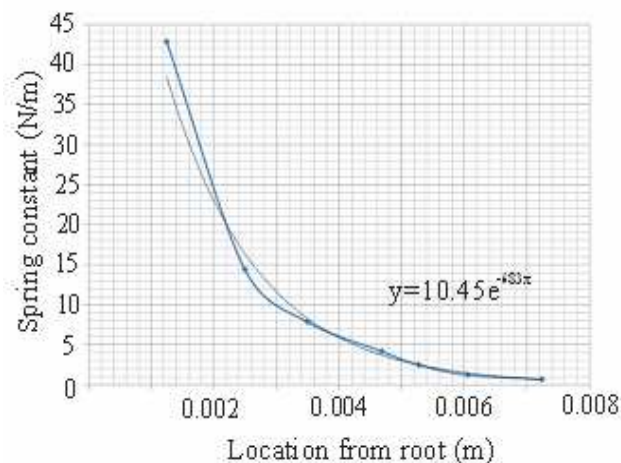


Figure 8: The distribution graph of spring constant in spanwise direction of *Calliphora* wing

The flexural stiffness for *Manduca Sexta* and *Aeshna Multicolor* obtained from the Finite Element Model by Combes and Daniel [2, 3] are approximately varies from 1×10^{-3} (near wing root) to 1×10^{-7} (near wing tip). The flexural stiffness that we defined from Figure 9 varies from 2.3×10^{-3} (near wing root) to 3.86×10^{-7} (near wing tip). However, bear in mind that the flexural stiffness is unique for every single insect but its trend is identical within the acceptable range.

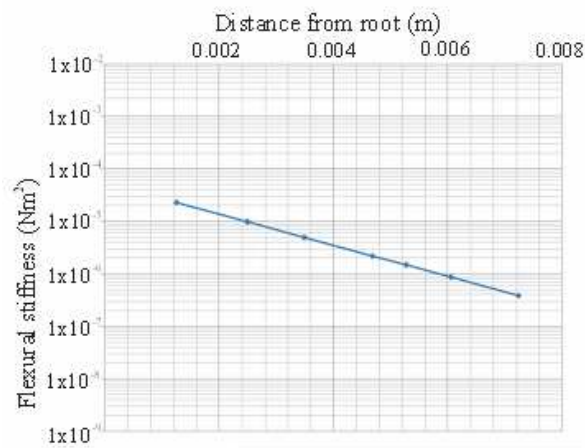


Figure 9: The distribution of flexural stiffness of the actual wing (EI) in spanwise direction

3.2 Aerodynamic forces

The Figure 10 is extremely important because they describe the aerodynamic forces (lift and drag) development depending on the situation with or without wing rotational circulation effect after the integration of the elementary forces. The aerodynamic forces have to be corrected and scaled with the body (isolated equally to both of the wing) because it also effects the development of total aerodynamic force indirectly particularly for hovering operation where the production of the total force is more obvious. As expected before, the lift and the drag force would jump to the maximum values just before and after the wing stroke reversal and turn to the minimum points during the mid stroke or even more during the stroke reversal. The maximum values of lift force range between 3.75×10^{-4} N up to 4.4×10^{-4} N whereas the drag force varies between 4×10^{-4} N and 6.5×10^{-4} N.

The Figure 11 explains about the resultant aerodynamic force obtained due to lift and drag force after the integration of the elementary forces. The resultant force is defined as the summation of square lift and drag and in this case the force enhancement effect is vital especially a couple milliseconds before and after the stroke reversal. They contribute to the resultant force growth up to 7×10^{-4} N.

3.3 Inertial forces

According to the Figure 12, the maximum values of horizontal inertial force peak are approximately equal to 4.2×10^{-3} N. The horizontal inertial force jumps to the maximum value during the stroke reversal when the wing actively accelerates or decelerates in arbitrary directions. Another issue that can be greatly discussed here is the peak force values during the front and back stroke reversal. Even though the range of the stroke reversal is different, but the amount of acceleration applied is almost the same. Therefore, the maximum amount of force developed during the front and back wing stroke reversal can be constantly obtained.

On the other hand, the maximum values of vertical inertial force peak are approximately 1.75×10^{-3} N. Again, it clearly shows that the wing actively accelerate and decelerate a couple millisecond before and after the stroke reversal. Meanwhile, the difference between the maximum and the minimum amount of peak force developed for each stroke is approximately 0.2×10^{-3} N where the front stroke reversal contributes a greater amount of vertical inertial force than the back stroke reversal. The other peak forces generated in this modeling execution are 1.19×10^{-3} N, 1.29×10^{-3} N and 1.59×10^{-3} N.

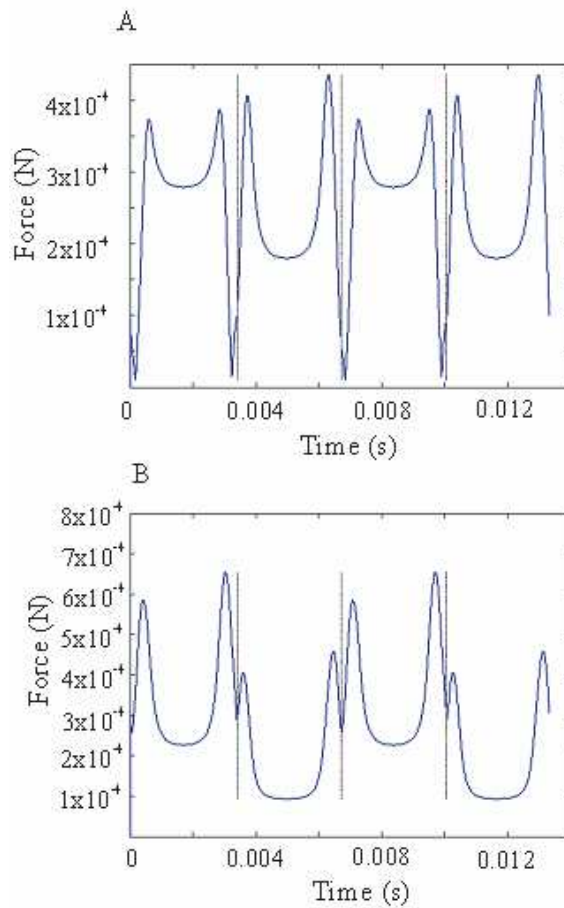


Figure 10: (A) Lift force in time domain for two wing strokes. (B) Drag force in time domain for two wing strokes

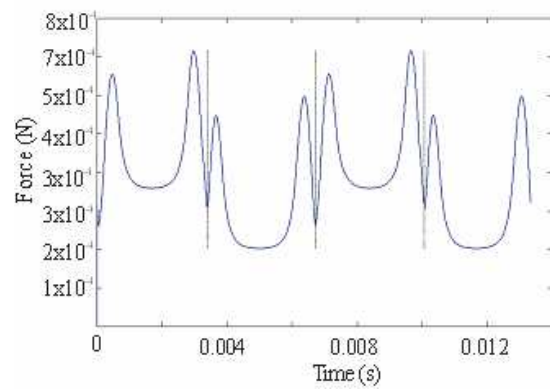


Figure 11: The resultant aerodynamic force in time domain for two wing strokes

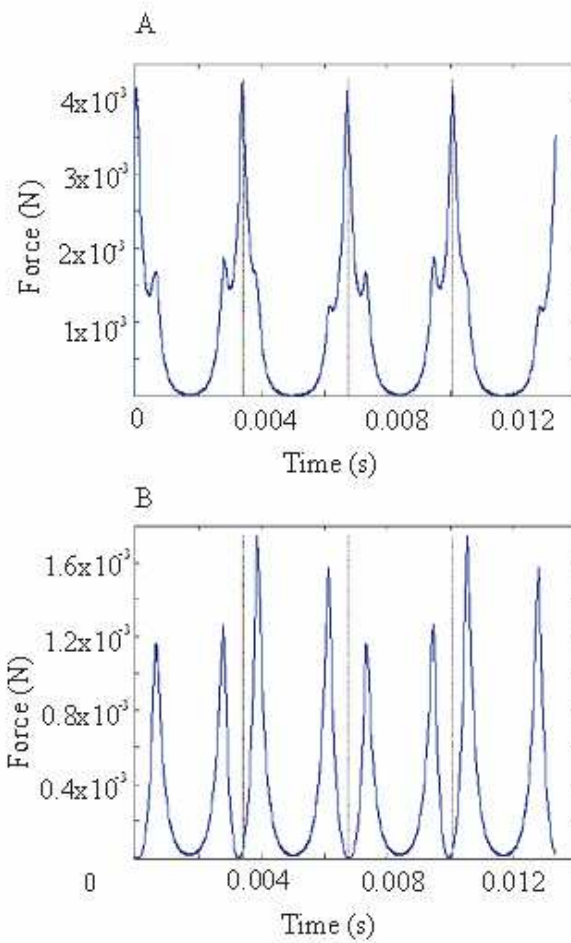


Figure 12: (A) Inertia force in horizontal direction. (B) Inertia force in vertical direction

3.4 Secondary forces

The Figure 13 explains all the operating secondary forces which are added mass and Magnus force. The highest peak of the Magnus force is approximately about 6.5×10^{-6} N and it clearly shows that the amount of force produced is not significant compared to the rest of forces listed before. Again, the vertical dash line will indicate the location of wing stroke reversal occurred. Accordingly, the peak of Magnus force formed during the back wing stroke reversal is a little bit lower than the front wing stroke reversal in approximately 1×10^{-6} N of increment. This situation since the range of wing rotation angle on both side of wing stroke reversal is different respectively. Likewise, the added mass effect produce several peaks to indicate the amount of force developed. Generally, the peaks of added mass effect vary between 0.6×10^{-4} N to 2.1×10^{-4} N.

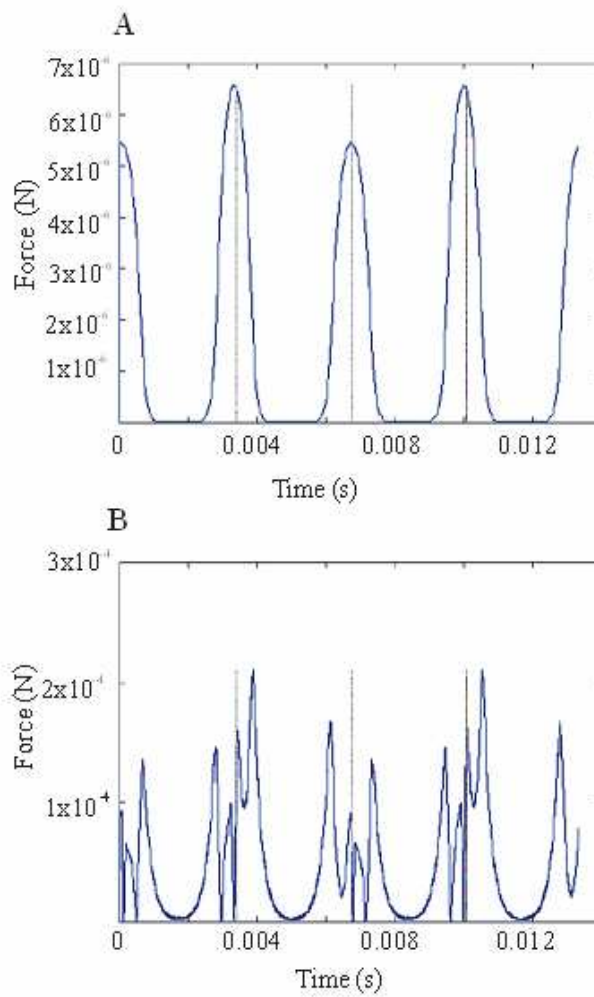


Figure 13: The Magnus force (A) and added mass effect (B) produced by the *Calliphora* operating in ambient air.

Figure 14 presented above is a compilation of all the forces obtain from the previous analysis. Horizontal inertial force is the one that will dominate with respect with others at maximum value of 4.25×10^{-3} N. Next, it follows by the vertical inertial force which mostly cause by the wing rotation at maximum value of approximately 1.2×10^{-3} N. Up to this stage, it is clearly stated that inertial force is the most influence force that later will plays an important role in the wing deformation. Furthermore, aerodynamic force stays in the third place in term of priority at the peak values of 0.7×10^{-3} N which are more or less 6 times smaller than the inertial effect. Added mass effect stays in ranking four, respectively. However, it may change depending on the ambient environment and certain situation. According to the graph, conclusion can be made that Magnus force effect is not significant and relevant in this situation and can simply be ignored. Last but not least, bear in mind that this standing will never be the same especially when the environment change as explained before.

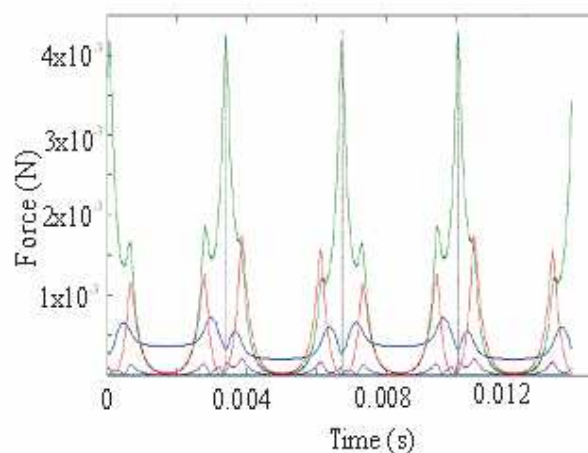


Figure 14: A clear view of all the reacted forces on the flapping insect of *Calliphora* affected by the change of surroundings for instance, air density. (Aerodynamic force noted by blue line, horizontal inertial force noted by dark green line, vertical inertial force noted by red line, Magnus force noted by light green line, added mass effect noted by pink line)

3.5 Forces integration

The following Figure 15 describes the result obtained on the compilation of the force in the horizontal direction. The maximum values of horizontal resultant force peak are approximately equal to 4.5×10^{-3} N. As a whole, horizontal resultant effect is strongly rely upon the rapid acceleration and deceleration of the wing stroke before it settle down during the midstrokes and turn almost to minimum amount of force (almost zero) as the wing steadily move at constant velocity.

The following Figure 16 describes the amount of resultant force in vertical direction given by the listed formula. There are four different peaks produced near the wing stroke reversal. The backstroke reversal produced approximately 2.1×10^{-3} N at the peak point while the lowest peak roughly about 1.6×10^{-3} N. On

the other hand, the resultant force in vertical direction at front stroke reversal is slightly higher than the previous backstroke reversal. Those peak forces near the front stroke reversal are 2.25×10^{-3} N of the highest point and 1.75×10^{-3} N respectively. In addition, during the mid stroke wing produce approximately about 0.25×10^{-3} N vertical resultant force. However, it is good to emphasize that all the peak of those forces are not exactly located at the wing stroke reversal line but it stands closer to that particular indication line.

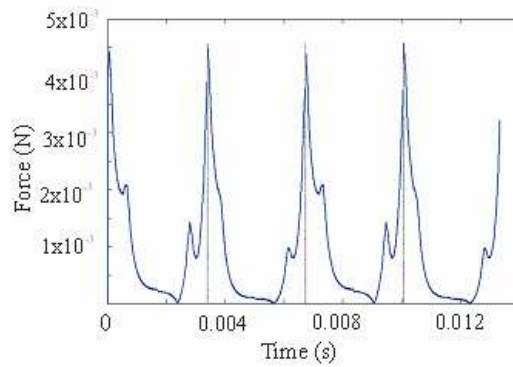


Figure 15: Resultant force in the horizontal direction

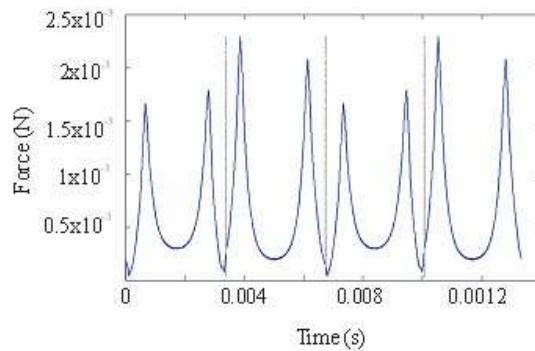


Figure 16: Resultant force in the vertical direction

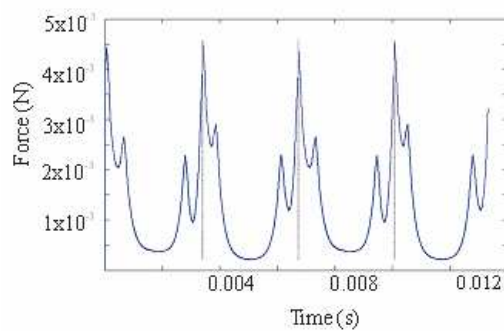


Figure 17: Total resultant force

The following Figure 17 explain about the amount of total resultant force produced from the given formula or in simpler means this total resultant force is generated from the resultant force in horizontal and vertical direction. This is the most accurate and precise force that we can use to calculate the degree of wing deformation in further chapters.

According to Figure 17, the peak point of resultant force is located exactly at wing stroke reversal line which is around 4.5×10^{-3} N and the force produced during mid stroke is only about 0.5×10^{-3} N. There are several peaks scattered just before and after that point.

3.6 Wing deformation

Figure 18 displays below describe the deflection characteristic of the wing at wing tip subjected to various different forces. The wing deflection calculated based on effect of the aerodynamic force, inertial force and most the important one, resultant force. According to the graph, the peak amount of deflection of the wing at tip due to aerodynamic force is approximately 3×10^{-4} m. Besides, the peak amount of deflection of the wing at tip due to inertial force is approximately 6.4×10^{-4} m. Furthermore, the peak amount of deflection of the wing at tip due to resultant force is approximately 1.35×10^{-3} m and. It is clearly shows that, the resultant force will be able to cause approximately 17% deflection at tip with respect to the wing length where the maximum deflection occurs at the wing stroke reversal. Bear in mind that the calculations of the wing deflection are strongly rely upon the location and also the force distribution.

Furthermore, in Figure 19 displays the wing angle deflection calculated based on effect of the aerodynamic force, inertial force and most the vital one, resultant force. According to the graph, the peak amount of deflection angle of the wing at tip due to aerodynamic force is approximately 2.2 degree. Besides, the peak amount of deflection angle of the wing at tip due to inertial force is approximately about 4.5 degree and the peak amount of deflection angle of the wing at tip due to resultant force is approximately 9.5 degree.

Subsequently, the Figure 20 describes the elastic potential energy characteristic of the wing exerted to various different forces. The wing elastic potential energy calculated based on the effect of the aerodynamic force, inertial force and most important one, resultant force. According to the graph, the highest peak of elastic potential energy of the wing at tip due to aerodynamic force is approximately about 1.55×10^{-8} J. Besides, the highest peak of elastic potential energy of the wing at tip due to inertial force is approximately about 6.5×10^{-8} J and the peak amount of elastic potential energy at tip due to resultant force is approximately about 3.2×10^{-6} J. Again, bear in mind that the calculations of the elastic potential energy are strongly rely upon the location and also the force distribution.

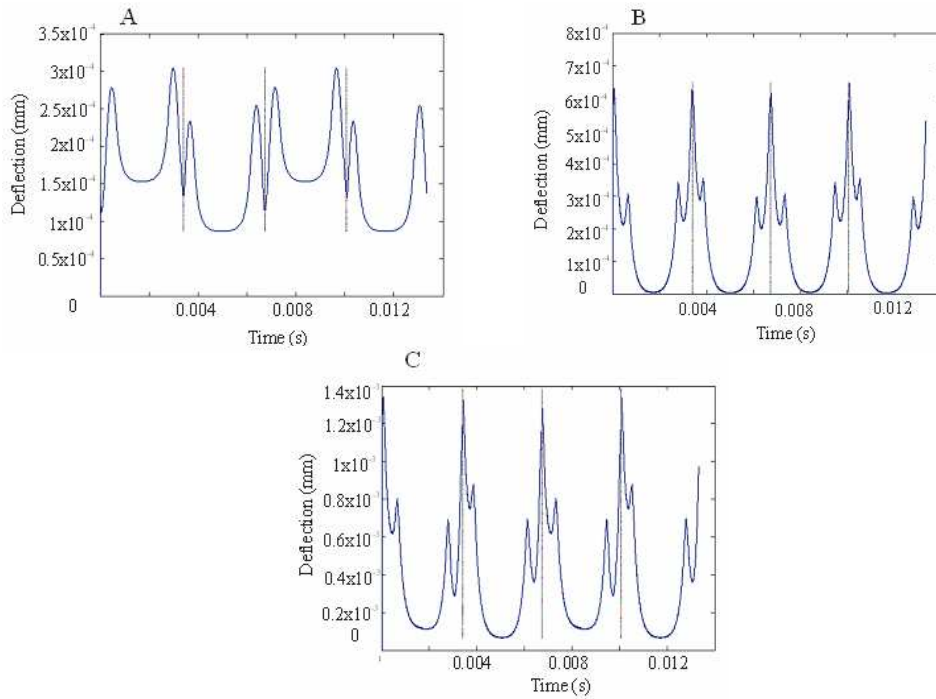


Figure 18: Wing tip deflection due to various forces (A), due to aerodynamic force, (B) due to inertial force. (C) due to resultant force.

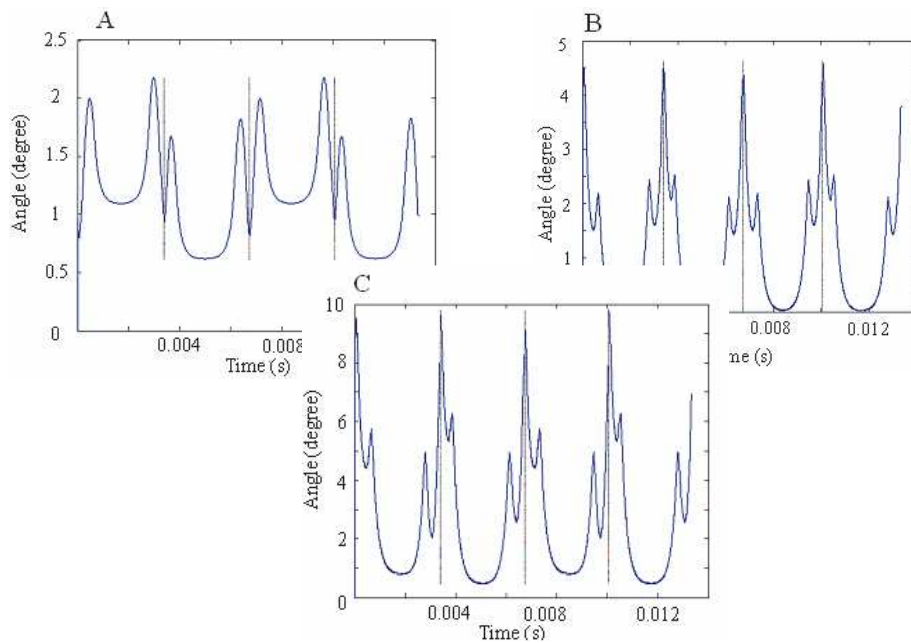


Figure 19: Wing tip deflection angle due to various forces (A), due to aerodynamic force, (B) due to inertial force. (C) due to resultant force.

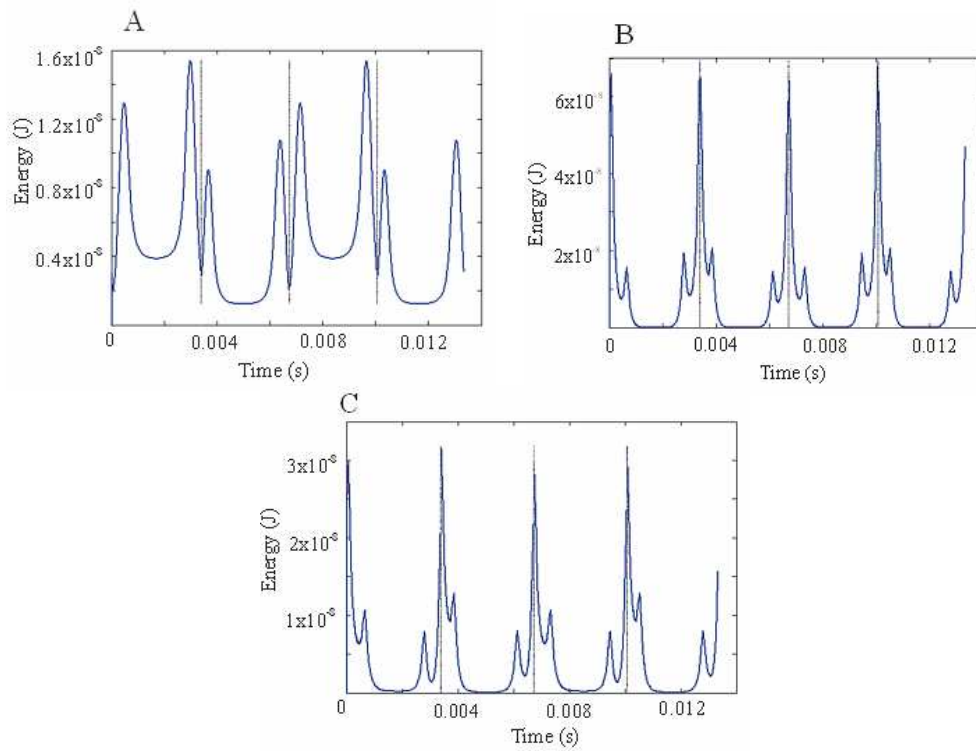


Figure 20: Elastic potential energy of the wing tip deflection due to various forces (A), due to aerodynamic force, (B) due to inertial force. (C) due to resultant force.

4.0 DISCUSSION

4.1 Flexural stiffness

For the system that obeys Hooke's Law the extension produced is directly proportional to the load exerted or deforming force. Under this condition, the object returns to the original shape and size after the load is removed. From the Figure 8, the trend line of the spring constant and the distribution of stiffness can be specified by approximating the relevant equation. The spring constant obtained is;

$$k = 90.45^{-6.83x} \quad (16)$$

The Figure 9 shows the distribution of the flexural stiffness in spanwise direction for *Calliphora's* wing obtained from the displacement of the wing localized for each section. Moreover, the graph displayed an evidence to validate the flexural stiffness data observed before by Combes and Daniel [8, 9] even though the flapping insects used are not in the same species, still they can be a good guidance to ensure our observation are heading towards appropriate direction.

4.2 Aerodynamic forces

The rotation circulation effect is a unique phenomenon that can only happen in flapping and rotating object which encourages boosting up the aerodynamic force generation during the stroke reversal. The location of stroke reversal can be easily defined as the vertical line plotted in both graphs. Furthermore the vertical line plotted in the total lift force graph described the mean lift produced during each stroke. According to the results, the wings actively accelerate and decelerate a couple milliseconds before and after the stroke reversal. Nevertheless, obviously during the mid stroke and the stroke reversal, the lift and the drag force jump to the minimum value. This result is extremely superior to support the idea presented by the previous researchers that the rotational effect enhance the aerodynamic performance near the wing stroke reversal

In other words, rotational circulation occurs during the transition of the pronation and supination because we can see the two peaks located near the wing stroke reversal where starting peak is less than the subsequent peak. But bear in mind, this percentage only relevant at certain situation, wing frequency and its shape. The difference of these two effects can be more significant for higher frequency and bigger wing size.

4.3 Inertial forces

The inertial force proves its value is approximately 6.4 times higher than the aerodynamic force during stroke reversal. As a whole, horizontal inertial effect is strongly rely upon the rapid acceleration and deceleration of the wing stroke reversal before it settle down during the midstrokes and turn almost to minimum amount of force (almost zero) as the wing steadily move at constant velocity.

On the other hand, the vertical inertial force also jumps to maximum value just before and after the stroke reversal and turn to minimum point exactly during the stroke reversal. However, it is clearly that during the mid stroke and the stroke reversal, the vertical inertial force is approximately equal to zero. During the stroke reversal, the wing rotates steadily at zero acceleration whereas during the mid stroke, the wing moves without any speeding up. Contrarily, with respect to the horizontal inertial force, the magnitudes of the peak vertical inertial force are inconsistent but it is still symmetry in shape for each stroke.

In the spanwise direction, the inertial effect decrease rapidly towards the wing tip and this can be predicted prior the analysis based on the information given by the graph of mass distribution because it concentrated near the wing root. However, it is not fully guaranty because the strips distance from the root also proportional to the inertial force. Unsurprisingly, this might be one of the appropriate reasons to explain why the insect's wing is thicker at the wing root. The mass concentrated at the wing root to the higher bending moment while the outer parts are lighter to reduce the stress due to high inertial affect at the wing base and to reduce the energy expenditure in the accelerating wing.

4.4 Secondary forces

According to the graph, the Magnus force is only important during the wing stroke reversal but it is still insignificant compared to the rest of forces involved because

the value is very small. It happens because the wing is actively rotate during the wing stroke reversal. As explained before that any rotating mechanisms will be a reason why the Magnus force established. Indeed, for this type of operating environment, the Magnus force is not significant or it can simply be ignored due to the normal air operating condition. As usual, nothing happen during the midstroke where amount of Magnus force produced is too little force to be considered and acknowledged.

Furthermore, several peaks scattered show the development of added mass effect but most of them concentrated before and after the wing stroke reversal in both side. Even tough, they are not as high as the aerodynamic force and inertial force but they are still significant in this kind of working environment. As usual, nothing happen during the midstroke where amount of added mass effect are almost disappeared and insignificant.

4.5 Wing deformation

The degree and the significance of the wing deflection are strongly relying upon the way that we distribute the elemental forces. Most of the wing deformations occur during the wing stroke reversal and approximately there is nothing happen during mid stroke because most of the forces occupied perform as the wing changes the stroke direction. Possibly, small deformation can be obtained during the mid stroke but the magnitude is too small and insignificant compared to the situation during the wing stroke reversal. Nonetheless, from the previous result displayed, we noticed that the inertial force is the most significant cause that produced wing deformation with respect to aerodynamic force. Moreover, this characteristic of the wing deformation will never be the same because of the changes in operating environment, wing size and its stiffness, kinematics used and so on will be able to contribute to changes. The simulation model is certainly an aid tool that can determine the effect of the changes means previously.

4.6 Concluding of remarks

A MATLAB modeling simulation is performed on the flapping wing of hovering namely blowfly (*Calliphora Vicina*). The forces around its body have to be understood especially on the influence of several kinematics variables such as frequency, mode of kinematic, stroke and rotation amplitude and so on. Then, all the forces obtained will be compiled in term of magnitude and direction in a single total force namely resultant force. This resultant force is beneficial for the computation of the characteristics of the wing deformation in several aspects of aerodynamic force, inertial force, Magnus force and added mass effect. As a final point, the vital issue has to be answered is how critical is the wing deformation due to these forces.

Prior the analysis of the characteristics of the wing deformation, the primary structural properties of the wing called flexural stiffness has to be observed experimentally by modeling the wing as a cantilever beam. The flexural stiffness of the wing is relying upon the topology of the veins and the joints because both of them will influence the wing rigidity and elasticity by performing as potential elastic energy storage. The most important outcomes obtained are the equation

that described the distribution of the wing stiffness in spanwise direction is exponentially decayed towards the wing tips. The wing flexural stiffness concentrated near the wing root and it describes that most of the forces exerted are damp by the region near the wing base. Finally the distribution of the wing flexural stiffness varies uniquely from 2.3×10^{-5} (near wing root) to 3.86×10^{-7} (near wing tip).

Another variable that may influence the wing deformation is the kinematics used. All the kinematics stated before are featured by the stroke angle, rotation angle and heaving angle. From this matter, the conclusion drawn is the angular velocity and acceleration of the wing stroke or rotation caused by a sharp or blunt wing turn is vital issues that influence the forces production. Furthermore, the angular acceleration is also crucial for the analysis of wing inertial effect in both direction of horizontal and vertical axis.

The next subject that has been discussed is the computation and formulation of the aerodynamic force which involve the lift and the drag force. As the wing modeled as a dynamic object, the involvement of the Kutta condition, Kramer effect due to wing rotation and also the Magnus effect had been elaborated. The aerodynamic force then can be distributed in several elements from the wing root to the wing tip according to the distribution of the chord length in spanwise direction.

As a conclusion, several statements have been produced such as most of the forces hit the maximum point at the wing stroke reversal whilst plunge to minimum level during the mid stroke. The wing stroke reversal is the most important features that enhance the performance of flapping flight of the insect. The rotational circulation effect enhance the generation of aerodynamic force at approximately 20% greater than it's absent at maximum affect.

The other issue that has been conferred in this study is the contribution of the inertial forces and the secondary forces which are include the Magnus force and added mass effect. The distribution of the wing mass is concentrated near the region of the wing root where the allocation of veins and joints are high caused a tremendous effect on the inertial force. Accordingly, the computation of the inertial force is directly proportional upon the magnitude of angular acceleration the wing stroke (horizontal inertial force) and the angular wing rotation (vertical inertial force). The conclusions that can be made from this concern is both of horizontal inertial force and Magnus force generate a maximum impact exactly during wing stroke reversal whereas the vertical inertial force and added mass effect hit the maximum contribution of force disperse near the wing stroke reversal. Besides, the amount of the horizontal force during the both wing stroke reversal is constantly in magnitude because it is only depending on the wing stroke amplitude.

Majority of the analysis that have been done are based on the certain amount of forces but it is not fully accurate because they will never act alone with any interaction with one another. For that reason, all the forces involved have to be integrated and associated in term of direction and magnitude as a single resultant force namely resultant force that will be use for the calculation of the wing deformation. Furthermore, the wing deflection will caused the subjected structure to deform and store some sort of potential energy called elastic potential energy

that will be able to bring back the wing to the original configuration. According to this analysis, several conclusions have been defined such as the horizontal inertial force is the highest force that will involved in the wing deformation, follows with the vertical inertial force, aerodynamic force, added mass effect and lastly the Magnus force. According to the analysis, the wing tip will be able to deflect up to 17% with respect to the wing length, at 9.5 degrees and stored approximately at 3.2×10^{-6} J of the elastic potential energy.

LIST OF SYMBOLS

α	Wing rotation angle
$\dot{\alpha}$	Wing rotation angular velocity
$\ddot{\alpha}$	Wing rotation angular acceleration
β_n	Added mass coefficient
c	Wing chord
dD	Elementary drag force
$d\delta_n$	Elementary wing deflection
dE	Elementary wing potential energy
dF_A	Elementary aerodynamic force
dF_{Av}	Elementary aerodynamic force in vertical direction
dF_a	Elementary added mass effect
dF_h	Elementary inertial force in the horizontal direction
dF_{Th}	Elementary total force in the horizontal direction
dF_{Tv}	Elementary total force in the vertical direction
dF_{Tr}	Elementary resultant force of the total force
dF_m	Elementary Magnus force
dF_v	Elementary inertial force in the vertical direction
dk	Elementary wing spring constant
dL	Elementary lift force
dm_w	Elementary mass of the strip
\hat{l}_x	Arm length x -axis
\hat{l}_x	Non-dimensional radial position along wing span
\hat{l}_y	Arm length in y -axis
n	Number of strip (element)
ϕ	Wing stroke angle
$\ddot{\phi}$	Wing stroke angular acceleration
ρ	Air density

R	Wing length
t	Time
\dot{v}_n	First derivative of normal velocity of wing element

REFERENCES

1. Ennos, A.R., 1988, 'The Inertial Cause of Wing Rotation in Diptera', *The Journal of Experimental Biology*, 1401, 161-169.
2. Dickinson, M.H, Lehmann, F.O. and Sane, S.P., 1999, 'Wing Rotation and the Aerodynamic Basis of Insect Flight', *Research Articles, Science - www.sciencemag.org*, 2841, 1954-1960.
3. Grodnitsky, D.L., 1999, 'Form and Function of Insect Wings: The Evolution of Biological Structures', *The John Hopkins University Press*, ISBN 0-8018-6003-2.
4. Pfau H.K., 1986, 'Untersuchungen zur Konstruktion, Funktion und Evolution de Flugapparates de Libellen (Insecta, Odonata)', *Tijdschr.Entomol*, 1293, 35-123.
5. Neville A.C., 1960, 'Aspect of the flight mechanics on anisopterous dragonflies', *The Journal of Experimental Biology*, 37, 631-656.
6. Hepburn, H.R. and Chander, H.D, 1976, 'Material properties of arthropod cuticles: The arthroal membranes', *J. Comp. Physiol*, 109, 177-198.
7. Ellington, C.P., 1984, 'The aerodynamics of hovering insect flight', *Phi. Tran. Roy. Soc. London*, 305, 1-180.
8. Combes, S.A. and Daniel, T.L., 2003a, 'Flexural stiffness in insect wings I. Scaling and the influence of wing venation', *The Journal of Experimental Biology*, 2061, 2979-2987.
9. Combes, S.A. and Daniel, T.L., 2003b, 'Flexural stiffness in insect wings II. Spatial distribution and dynamic wing bending', *The Journal of Experimental Biology*, 2061, 2989-2997.
10. Ganguli, R. Lehmann, F.O. and Gorb, S., 2008, 49th AIAA/ASME/ASCE/AHS/ASC Structures, *Structural Dynamics and Materials Conference*, 7-10 April 2008, Schaumburg, Illinois, USA
11. Walker, J.A., 2002, 'Rotational lift: something different or more of the same', *The Journal of Experimental Biology*, 2051, 3783-3792.
12. Dickinson, M.H, 1996, 'Unsteady mechanism of force generation in aquatic and aerial locomotion', *Am. Zool.*, 366, 537-540
13. Sane, S.P., 2003, 'The aerodynamics of insect flight', *The Journal of Experimental Biology*, 2061, 4191-4208.
14. Dickinson, M.H, Lehmann F.O. and Gotz, K.G., 1993, 'The active control of wing rotation by *Drosophila*', *The Journal of Experimental Biology*, 182, 173-189.
15. Shvets A.I., Zakharenkov M.N., Osimin, P.K., 1979, 'Otchet Instituta Mekhaniki MGU', *Report of the Moscow University Institute of Mechanics*.